Environ. Eng. Res. 2017; 22(1): 75-86
https://doi.org/10.4491/eer.2016.080

pISSN 1226-1025
eISSN 2005-968X

Investigations on aerosols transport over micro- and macro-scale settings of West Africa

Moses Eterigho Emetere†

Department of Physics, Covenant University Canaan land, P.M.B 1023, Ota 122333, Nigeria

ABSTRACT

The aerosol content dynamics in a virtual system were investigated. The outcome was extended to monitor the mean concentration diffusion of aerosols in a predefined macro and micro scale. The data set used were wind data set from the automatic weather station; satellite data set from Total Ozone Mapping Spectrometer aerosol index and multi-angle imaging spectroradiometer; ground data set from Aerosol robotic network. The maximum speed of the macro scale (West Africa) was less than 4.4 m/s. This low speed enables the pollutants to acquire maximum range of about 15 km. The heterogeneous nature of aerosols layer in the West African atmosphere creates strange transport pattern caused by multiple refractivity. It is believed that the multiple refractive concepts inhibit aerosol optical depth data retrieval. It was also discovered that the build-up of the purported strange transport pattern with time has enormous potential to influence higher degrees of climatic change in the long term. Even when the African Easterly Jet drives the aerosols layer at about 10 m/s, the interacting layers of aerosols are compelled to mitigate its speed to about 4.2 m/s (macro scale level) and boost its speed to 30 m/s on the micro scale level. Mean concentration diffusion of aerosols was higher in the micro scale than the macro scale level. The minimum aerosol content dynamics for non-decaying, logarithmic decay and exponential decay particulates dispersion is given as 4, 1.4 and 0 respectively.

Keywords: Aerosols, Computational simulation, Ewekoro, Macro-scale, Micro-scale, West Africa

1. Introduction

Aerosols transport is largely dependent on the meteorological conditions over a geographical location. The meteorological conditions influence the kind of emission, particulates mixing rates, particulate deposition or decay rates and the type of dispersion [1-3]. The mathematical representations of the meteorological influence are complex because the menace of climate change has greatly affected the global energy budget. Hence, modelling aerosols transport over the atmospheric space of any geographical location requires an in-depth understanding of salient meteorological factors which may be very difficult to express analytically [3, 4]. Before now, numerical models were used to describe aerosols transport. For example, PSU/NCAR mesoscale model MM5 was used to monitor dusts transport. This was possible because the study focussed on the strong northerly wind in the planetary boundary layer (PBL).

The analytical study can be developed by considering salient meteorological parameters required to determine aerosols transport. Sun et al. [4] showed the difficulties of simulating the evolution of weather systems with respect to its wind fields that controls aerosol transport in the PBL. In like manner, aerosols transport in the troposphere can be explained upon salient indicators such as wind properties, precipitation, mixing, tuning constant, aerosol lifetime which makes up the viscosity of the atmosphere, etc.

The summation of necessary indicators in form of a comprehensive numerical model is not adequate because basic errors in the mathematical expression are difficult to screen-out in a numerical model [5]. Some numerical models have used the semi-Lagrangian scheme to address the momentum, energy, and mass conservation [6]. In characterizing the aerosol transport, Gazala et al. [7] gave an assumption that the Total Ozone Mapping Spectrometer (TOMS) aerosol index (AI) is proportional to the dust burden and optical depth. This assumption was duplicated by Wen et al. [8] who developed a 4-D Purdue Regional Climate Model (PRCM) which characterized the evolution of the interaction between weather and dusts. How much has the numerical model

Received June 12, 2016 **Accepted** October 17, 2016

† Corresponding author
Email: moses.emetere@covenantuniversity.edu.ng
Tel: +234-8035267598

solved the aerosols transport pattern in an active PBL?

The importance of numerical models in interpreting atmospheric measurement cannot be overemphasized because it is a tool which simplify as well as elaborate the anomalies of direct measurements. Since the characteristic of a good model is its ability to examine the micro or macro-scale transport or both transport scale within a predetermined geographical region. The use of pure numerical model would be grossly inadequate to accommodate the flexibility of changing parameters in the lower atmosphere i.e. when models are applied to dissimilar geographical region. For example, the fractional advection-dispersion equation (FADE) has shown perfection in describing micro-scale conditions but showed imperfection to describe macro-scale conditions [9].

The deficiency of the MM5 model is its incorrect representation and unrealistic simplification of marine boundary layer thermodynamics over water bodies [10]. This singular deficiency leads to the overestimation of the sensible and latent heat fluxes over the water bodies or surface. Though the modified MM5 model is adjudged accurate [11], the complexity of the West African atmosphere i.e. the north-east wind influence was not figured into the modified model. As mentioned earlier, the major challenge confronting air quality models are its ability to operate within the macro scale and micro scale framework of a regional model. This quality strengthens the results and judgments of forecasting pollution events within regional models. Very few numerical models satisfy this basic requirement. This has led to the call for several improvements in the secondary requirements for developing (particle formation, mixing and decay rate) numerical models [12]. In this study, we propose an analytical solution which accommodates meaningful modification in the future.

Taking a cue from literature, the aerosols optical properties are sensitive to the size distribution over an area. Also, the chemical composition depends on the relative humidity over geographical area [13]. To solve the challenge of aerosol size distribution, we developed the aerosol model which comprises of salient meteorological factors [14]. The outcome adequately mimicked the satellite and ground aerosol imagery on a macro-scale. It showed success also on the meso-scale but not on a micro-scale. This major defect is seen in other numerical models like the Community Multiscale Air Quality (CMAQ). Hence, the need to develop a model that would adequately capture the physics of aerosol transport in the atmosphere on a micro-scale or macro-scale level is necessary for accurate computational task. To adequately develop an efficient technique for solving aerosols transport pattern/feature over a geographical region, it is important to examine the West African climate system.

The climate system of West Africa (WA) is unique compared to other climatic regions. WA climate is majorly tropical. The far northern portion of WA is arid and stretches-out into the Sahara desert. The climatic zones of WA are shown in Fig. 1. The four different climatic zones in WA are Sahelian zone, Sudano-Sahelian zone, Sudanian zone and Guinean zone. Sahelian zone is a region of perennial vegetation, the average annual precipitation ranges between 250 mm and 500 mm. The Sahel zone is dominated by the West Africa monsoon (WAM) which affects large-scale circulation of moisture from the Atlantic Ocean into the Sahel zone. The Sahel zone is also characterized by wind reversal in

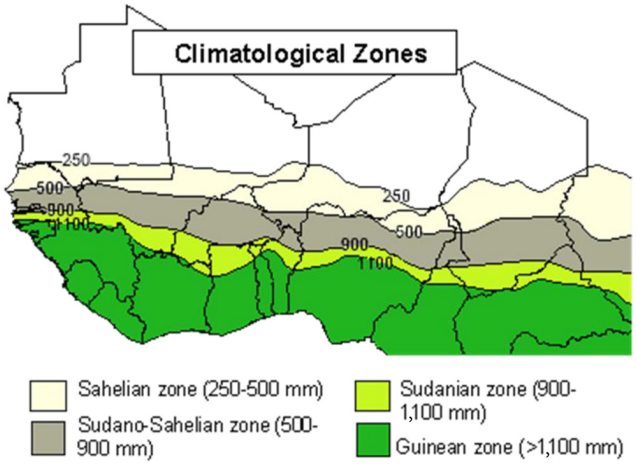

Fig. 1. Climatic zones in West Africa. Adopted from FAO.

the lower atmosphere. Sudano-Sahelian zone is a region where average annual precipitation ranges from 500 mm to 900 mm. Sudanian zone is a region of an average annual precipitation that ranges from 900 mm to 1,100 mm. Guinean zone is a region of an average annual precipitation exceeding 1,100 mm. Atmospheric circulation pattern in the four zones is controlled by some salient factors like African Easterly Jet (AEJ), Intertropical Convergence Zone (ITCZ), Intertropical Discontinuity (ITD), associated heat low (HL), Subtropical Jet (STJ), troughs and cyclonic centres associated with African Easterly Waves (AEW) and Tropical Easterly Jet (TEJ).

The objective of this paper is to show a well-defined aerosol dispersion could theoretically be used to validate aerosols transport both on the micro-scale and macro-scale platforms. In section two, the dispersion model was used to determine the aerosols content dynamics. The aerosols content dynamics is a salient component to study the aerosol transport in WA. The location of study and the measuring observations were described in section three and four respectively. In section five, the theory of the aerosols content dynamic was tested in a virtual system. The outcome was applied to the mean concentration diffusion over pre-defined micro scale enclave. In section six, the mean concentration diffusion over pre-defined macro scale enclave was described in details with the aid of satellite and ground observations.

2. Theoretical Background

Most aerosols transport originates from the lower atmosphere. The aerosols emission trend and transport over WA is largely dependent on anthropogenic activities and the dusty north-east winds. The pattern at which the dispersed aerosols diffuse into the atmosphere depends on myraids of factors that is largely localized to a particular geographical region. For example, the tropical region of WA is characterized by massive upradfts and wind recirculation at certain altitude. The mathematical representation of all the atmospheric factors that participates in aerosols transport may be challenging. More challenging is the accurate determination per time of each atmospheric factor engagement in a versed-dynam-

ic system. Hence, applying numerical models to solve atmospheric problem may be inadequate because of its generalized approach. The use of an analytical approach may be more flexible to incorporate salient discoveries to the already developed model whose governing advection dispersion flow equations are stated below [1-2]

$$\frac{\partial C}{\partial t}+V_x\frac{\partial C}{\partial x}-V_z\frac{\partial C}{\partial z}-V_y\frac{\partial C}{\partial y}=\frac{\partial}{\partial z}\left(K_z\frac{\partial C}{\partial z}\right)+\frac{\partial}{\partial y}\left(K_y\frac{\partial C}{\partial y}\right)+\frac{\partial}{\partial z}\left(K_{z2}\frac{\partial C}{\partial z}\right)+\frac{\partial}{\partial y}\left(K_{y2}\frac{\partial C}{\partial y}\right)-P+S \quad (1)$$

$$-V_z\frac{\partial C}{\partial z}=-\frac{\partial}{\partial z}\left(K_z\frac{\partial C}{\partial z}\right)+\frac{\partial}{\partial y}\left(K_y\frac{\partial C}{\partial y}\right) \quad (2)$$

$$V_x\frac{\partial C}{\partial x}=\frac{\partial}{\partial y}\left(K_{y2}\frac{\partial C}{\partial y}\right)-\frac{\partial}{\partial z}\left(K_{z2}\frac{\partial C}{\partial z}\right) \quad (3)$$

Here, V is the wind velocity (m/s), P is the air upthrust, x is the wind coordinate measured in wind direction from the source, y is the cross-wind coordinate direction, z is the vertical coordinate measured from the ground, C(x, y, z) is the mean concentration of diffusing pollutants of diffusing substance at a point (x, y, z) [kg/m^3], K_y, K_z are the eddy diffusivities in the direction of the y- and z- axes [m^2/s], S is the source/sink term [kg/m^3-s]. The aerosols transport do not always traverse the positive x, y and z axes, sometime due to recirculation, they traverse negative axes. Hence, the eddy diffusivity changes and carry a new value denoted as K_{z2} and K_{y2}. Therefore we propose that aerosols transports may possess two or more diffusivities.

The ascending particulate-mild dispersion shown in Eq. (2) and Eq. (3) are more appropriate to examine aerosols transport within the lower atmosphere [5]. For a trivial case, Eq. (2) can be solved- using separation of variable i.e. C(x, y, z) = A(x)B(y)Q(z) with the initial boundary conditions as A(0) = a; A^{I}(0) = 0; B(0) = a; B^{I}(0) = 0; Q(0) = b. The analytical solution can be done using any convenient mathematical technique. However, the 'separation of variable' technique was adopted on the grounds that the separate concentration A(x), B(y) and Q(z) along any of the axes could be monitored individually. It is proposed in this research that the idea of separating the components of the mean concentration of diffusing pollutants is very important for nowcast or forecast purposes.

On the assumption that k_y & k_z are constants, then

$$V_z\frac{\partial C}{\partial z}=\left(K_z\frac{\partial^2 C}{\partial z^2}\right)+\left(K_y\frac{\partial^2 C}{\partial y^2}\right)+\left(K_z\frac{\partial^2 C}{\partial x^2}\right) \quad (4)$$

Using separation of variable technique, C(x, y, z) = X(x)Y(y)Z(z)

$$V_zXYZ'=k_zXYZ''+k_yXY''Z+k_zX''YZ \quad (5)$$

Divide through by XYZ

$$V_z\frac{Z'}{Z}=k_z\frac{Z''}{Z}+k_y\frac{Y''}{Y}+k_z\frac{X''}{X} \quad (6)$$

Since Eq. (6) is a complex expression, it is assumed that the terms are individually equal to a constant.

$$V_z\frac{Z'}{Z}-k_z\frac{Z''}{Z}=\delta^2 \quad (7)$$

$$V_z\frac{Z'}{Z}-k_z\frac{Z''}{Z}-\delta^2=0 \quad (8)$$

$$k_y\frac{Y''}{Y}=\beta^2 \quad (9)$$

$$k_z\frac{X''}{X}=\gamma^2 \quad (10)$$

So that $\delta^2=\gamma^2+\beta^2$. Eq. (7)-(10) can be restructured with respect to diffusivity

$$k_zZ''-V_zZ'+\delta^2Z=0 \quad (11)$$

For V_z and k_z, the trial solution $Z=\exp(-pz)$ leads to

$$p=\frac{V_z\pm\sqrt{V_z^2-4k_z\delta^2}}{2k_z} \quad (12)$$

For $V_z\gg4k_z\alpha^2$, the solution becomes p = 0 and $p=\frac{V_z}{k_z}$

$$Y''-\frac{\beta^2}{k_y}Y=0 \quad (13)$$

$$X''-\frac{\gamma^2}{k_z}X=0 \quad (14)$$

Adopting the general solutions of $Z=A\exp(-pz)+C\exp(-pz)$, $X=A\sin\left(\frac{\gamma}{\sqrt{k_z}}x\right)+B\cos\left(\frac{\gamma}{\sqrt{k_z}}x\right)$ and $Y=C\sin\left(\frac{\beta^2}{\sqrt{k_y}}y\right)+D\cos\left(\frac{\beta^2}{\sqrt{k_y}}y\right)$ on the the initial boundary conditions that Y(π) = 0, X(π) = 0, Y(0) = 0, X(0) = 0. Then, π

$$Z=b\exp\left(-\frac{V_z}{k_z}z\right) \quad (15)$$

$$Y=a\cos\left(\frac{\beta}{\sqrt{k_y}}y\right) \quad (16)$$

$$X=a\cos\left(\frac{\gamma}{\sqrt{k_z}}x\right) \quad (17)$$

In the sedimentation of aerosols by ultrasounds, D and B shows the relation of amplitude of speed of the weighed particle to amplitude of speed of a particle of gas. Hence, $D = B = a$. Likewise, $C = b$. When the initial boundary condition is applied (Y(π) = 0, X(π) = 0), then $\frac{\beta}{\sqrt{k_y}}=\frac{n\pi}{2}$ or $\frac{\gamma}{\sqrt{k_z}}=\frac{n\pi}{2}$

Hence, the solution is given as

$$C(x,y,z)=a^2 b\cos\left(\frac{n\pi}{2}x+\eta\right)\cos\left(\frac{n\pi}{2}y+\xi\right)\exp\left(-\frac{V_z}{k_z}z\right) \quad (18)$$

a and b are numerical constants which typically refers to selected range and height respectively, n is the tuning constant η and ξ are phase difference that can be determined empirically via the incorporation of remotely sensed data set and Matlab curve tool [5]. The practical application of Eq. (18) is explained in the next session. Eq. (18) represents three occurrences i.e. sinusoidal flux of the aerosol content $\left(b\cos\left(\frac{n\pi}{2}x+\eta\right)\right)$, vertical profile of aerosol content $\left(a\cos\left(\frac{n\pi}{2}y+\xi\right)\right)$ and dynamics of the aerosol content $\left(\delta=a\left[\exp\left(-\frac{V_z}{k_z}z\right)\right]\right)$.

3. Materials and Methods

The location of study is illustrated in Table 1 below. Two sites were considered i.e. the micro-scale site [15] and macro-scale size [16]. The micro-scale site are two cement factories located five kilometers North of Ewekoro town (6°55′ N 3°12′ E/6.93°N3.21°E). Hence, Ewekoro was selected as a typical example of the micro-scale site because the pollution dispersion from both cement factories could be describe in term of non-decay, logarithmic decay and exponential decay type of dispersions. It is within the tropical rainforest belt of Ogun state, southwest-Nigeria. The topography of Ewekoro is classified as a southern upland [17]. It has an area of 594 km^2. The wind speed and direction was obtained from the Davis automatic weather station installed at Covenant University. The macro-scale site is the whole of the West African space. The satellite imagery used for this research was obtained from the TOMS AI observation for January of 2000-2003 of West

Table 1. Location of Study

Location	Geographical coordinates	Area (km^2)	Geographical features
Nigeria	Latitude 40°N - 140°N and longitude 30°E - 140°E	923,768	River Niger and Benue; Jos, Obudu and Mambilla Plateau; and Niger Delta, Ogun-Osun, Owena River basins, desert in the far north
Ghana	Latitude 8°N and longitude 12°W	238,533	plains, low hills, rivers, Lake Volta, ecoregions (coastline, sandy shore, scrub), plateau region (Kwahu Plateau and Ashanti uplands), mangroves
Togo	Latitude 8°N and longitude 1°10′E respectively	56,785	tidal flats, sandy beaches, shallow lagoons, lakes, etc.
Cape Verde	Latitude 14°55′N and longitude 23°31′W	4,033	comprise of arid Atlantic islands that are located off the west coast, landscape, volcanoes, cliffs, islands, islets, high mountains
Côte d'Ivoire	Latitude 5°N to 10°N and longitude 4°W to 6°W	322,463	plateau, tropical forest and coastal inland lagoons in the south
Liberia	Latitude 6°N and longitude 9°W	110,000	hilly terrain, low mountains and rolling plains and plateau
Sierra Leone	Latitude of 6°N and 9°N, and longitude of 11°W and 13°W	71,740	has four geographical regions; upland plateau, coastal Guinean mangroves, the wooded hill country, and the eastern mountains
Equatorial Guinea	Latitude 1°N to 3°N and longitude 8°E to 11°E	28,050	islands, volcanic formations, low hills
Guinea Bissau	Latitude 11°N to 12°N and longitude 14°W to 15°W	36,125	low coastal plain, Guinean mangroves, forest
Gambia	Latitude 13.2°N to 13.5°N and longitude 14°W to 16°W	11,295	River Gambia, sand cliffs, low Rocky Hills, mangrove swamp
Benin	Latitude 6°N to 11°N and longitude 1°E to 2°E	112,622	low-lying sandy coastal plain, mangroves, forest
Cameroon	Latitude 2°N to 12°N and longitude 9°E to 15°E	475,440	mountains, Central African mangroves, desert, plateau, tropical rain forest, savanna grassland, rivers and ocean coastland
Burkina Faso	Latitude 10°N to 14°N and longitude 0.7°W to 4°W	274,200	forests in the south, desert in the north
Mauritania	Latitude 16°N to 22°N and longitude 7°W to 17°W	1,030,700	arid plains, cliff, plateau, oases
Mali	Latitude 16°N to 22°N and longitude 7°W to 17°W	1,240,192	mainly desert
Guinea	Latitude 7°N to 12°N and longitude 8°W to 13°W	245,860	lowland, Guinean forest, highlands, south-eastern rain-forest region
Senegal	Latitude 12°N to 16°N and longitude 13°W to 17°W	196,190	foothills rise from the Sahel, Gambia River and Senegal River

Africa and multi-angle imaging spectroradiometer (MISR). The Earth Probe TOMS is no longer in use because its transmitter failed on December 2, 2006. MISR was launched in 1999 to measure the intensity of solar radiation reflected by the planetary surface and atmosphere. The MISR operates at various directions i.e. nine different angles (70.5°, 60°, 45.6°, 26.1°, 0°, 26.1°, 45.6°, 60°, 20.5°) and gathers data in four different spectral bands (blue, green, red, and near-infrared) of the solar spectrum. The blue band is at wavelength 443 nm, the green band is at wavelength 555 nm, the red band wavelength is at wavelength 670 nm and the infrared band is at wavelength 865 nm. MISR acquire images at two different levels of spatial resolution i.e. local and global mode. It gathers data at the local mode at 275 meter pixel size and 1.1 km at the global mode. Typically, the blue band is to analyze coastal and aerosol studies. The green band is to analyze Bathymetric mapping and estimating peak vegetation. The red band analyzes the variable vegetation slopes and the infrared band analyzes the biomass content and shorelines. The Aerosol robotic network (AERONET) program is a ground-based remote sensing aerosol networks established by NASA and PHOTONS. It provides globally distributed observations of spectral aerosol optical depth (AOD), inversion products, and perceptible water in diverse aerosol regimes. The simulation was carried out using the Matlab.

4. Results and Discussion

4.1. Verification of Model on a Micro Scale

A micro scale in this research is defined as the space within a near homogenous sub layer of the troposphere [18]. In this case, we consider the surface layer of the troposphere. Therefore, at layer 2 of the PBL (surface layer), the aerosols number density ranges between 140 cm^{-3} and 515 cm^{-3} in clean tropospheric air and polluted urban environments [19-20]. Hence, the aerosol content dynamics mimics the aerosol density distribution solution given by McKibbin [21] in Eq. (19). If 'a' in Eq. (18) is analyzed such that the vertical profiling is done with respect to time, then it is not a constant because of its transverse dispersion expressed in Marco et al. [22]. The translation of 'a' from a constant to variable is referred to as a particular case where the aerosols transport is within a confined micro-scale system in the Stokes' regime [23].

$$a = \frac{Q}{4\pi\sqrt{D_L D_T t^2}} \tag{19}$$

Here, Q is the mass of the particle released above the ground from the cement factory, D_L is the longitudinal dispersion coefficient, D_T is the transverse dispersion coefficient, t is the time taken for the aerosol to reside at each layer, V_x is the wind velocity (m/s) t is the time taken. In the mild diffusion region, $D_L = D_T$ because the particles becomes lighter and more energetic [24-25] and reaches its quasistationary level at about 10,000 s [26] before atmospheric blocking takes place [27]. Hence, Eq. (19) may be written as $a = \frac{Q}{4000\pi D_T}$, then

$$\delta = \frac{Q}{4000\pi D_T} exp\left(-\frac{V_z}{k_z} z\right) \tag{20}$$

From the refined Eq. (20), the wind velocity is a major function of the aerosol content dynamics (δ). The wind dynamics was harvested via the Davis Weather Station which was mounted about 1.2 km from the research site (cement factory). First, we determined the theoretical expectation of δ (Fig. 1-3) by assuming that the chunk of the mass of the particle released above the ground from the cement factory is about 4-10 kg within 1,000 s. Three cases were considered i.e. when the mass (Q) ejected do not decay (Fig. 3(a)), when the mass (Q) ejected has a logarithmic decay (Fig. 3(b)) and when the mass (Q) ejected has an exponential decay (Fig. 3(c)). The three conditions were adopted from Drewnick et al. [28] aerosol quantification where different atmospheric decay conditions were discussed.

When the mass ejected do not decay or vanish, the PBL experiences massive aerosol loading which increases linearly as shown in Fig. 3(a). This means that life forms are exposed to radiative heating effects which are as a result of either massive absorption or scattering of radiation from the sun by the aerosols. When the mass ejected are decaying exponentially or logarithmically, the aerosols loading in the PBL are reduced by rainfall or wind. However, the tendency of the aerosol loading to concentrate at specified sub-layer of the PBL e.g. surface layer may be enhanced by human activities. This possibility is represented in the term P & S in Eq. (1).

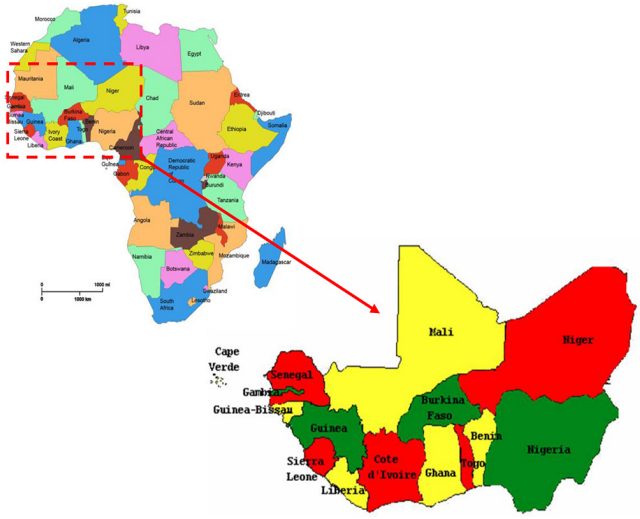

Fig. 2. Map of West Africa.

Table 2. Total Deposited Air Particles (source: Olaleye *et al.*,(2005))

	Experimental air deposition	Theoretical air deposition	% error
Alaguntan	23.51	23.27 (β = 30)	1.20
Itori	27.89	25.30 (β = 60)	9.20
Junior staff qtrs	10.35	10.34 (β = 40)	0.97
Olapeleke	15.84	12.75 (β = 5)	19.5
wasinmi	5.34	5.89 (β = 0)	10.2

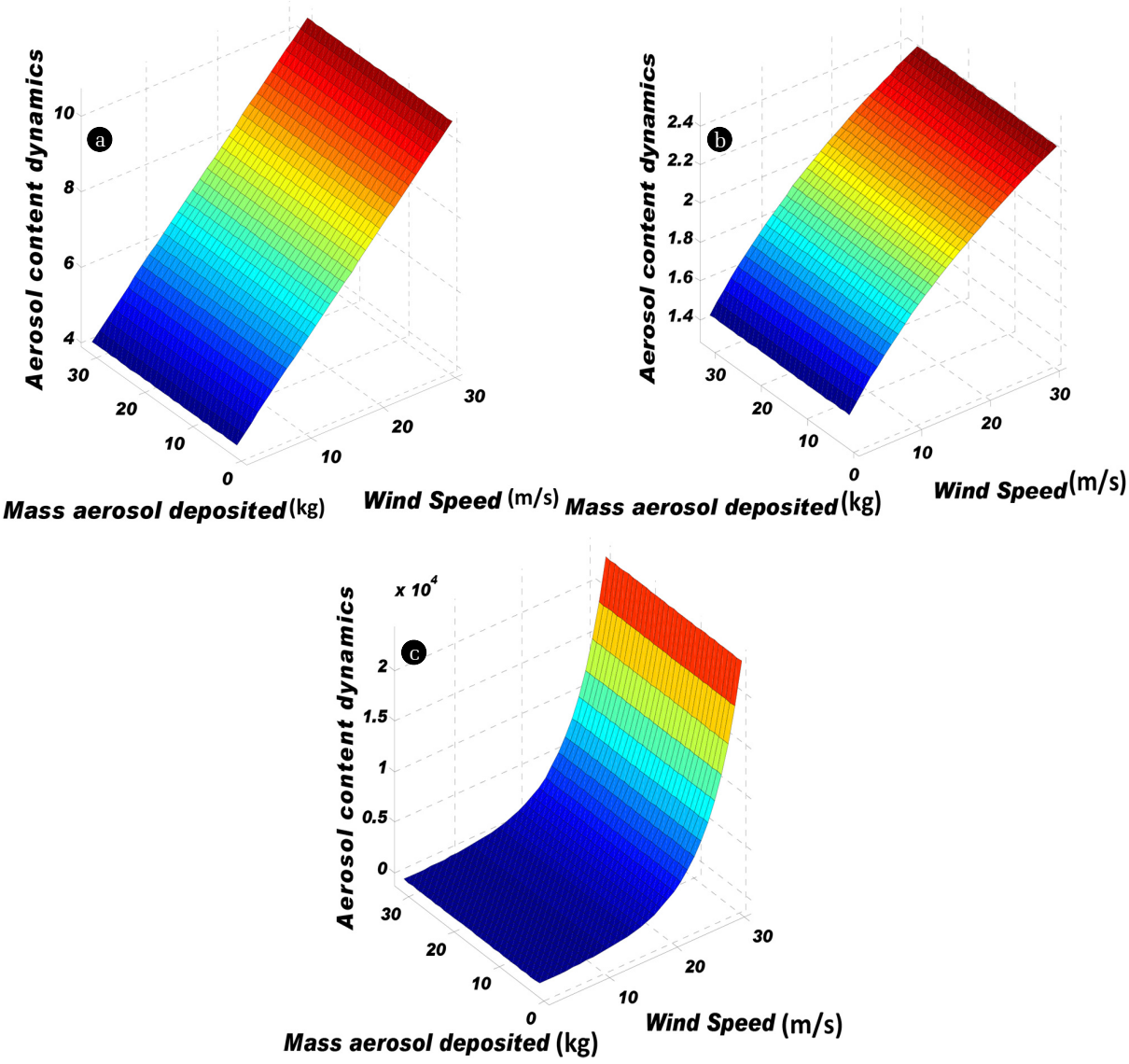

Fig. 3. (a) Mass (Q) ejected do not decay (b) Mass (Q) ejected have a logarithmic decay (c) Mass (Q) ejected have an exponential decay.

In the three cases illustrated in Fig. 3, the aerosol mass deposition is the most consistent parameter. Hence, the accuracy of the aerosol mass deposition was affirmed in Table 2 i.e. compared to the experimental air pollutants deposition at various sampling points reported by Olaleye *et al.* [29]. The aerosol content dynamics increases in magnitude in either of the cases mentioned earlier. This shows that the wind speed is the trigger for aerosol advection or deposition. We monitored the readings of both the wind speed and its direction for January (see Fig. 4). Fig. 4 is the wind speeds corresponding to the monthly averages. We harvested the first twenty events of the directional coordinates of the wind in the 1,200 s at various intervals. Recall that the Davis Pro II weather station was positioned at the surface layer of the PBL to see the effect of the wind speed on the aerosol content dynamics. The main characterization for standard divisions for the magnitude of wind

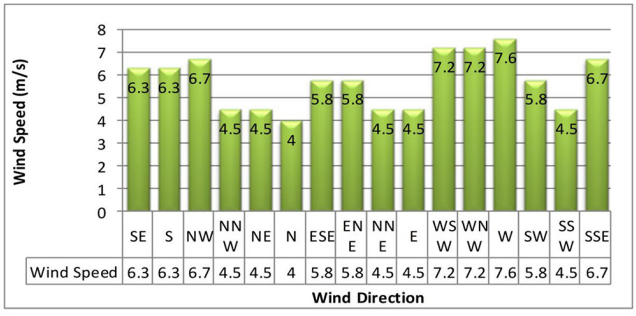

Fig. 4. Magnitude of wind speed within different directions.

speed within different directions over the research region has been reported in [30]. The wind speed in January showed greater tendency

to transverse the west-south-west (WSW) or south-west-west (SWW). From Fig. 4, the wind speed at WSW is high and has more consistent trend than other wind directions. Other coordinates i.e. SW or S exhibit inadequate trend. Hence, it supports few abnormalities observed in Table 2. Therefore, the three dimensional semi-plume model determines rather the deposition points and two dimensional semi- plume model determines the wind field dynamics. Therefore, the solution to controlling the flow of air pollutants from any anthropogenic sources is illustrated through the mathematical model in Eq. (4).

4.2. Verification of Model on a Macro Scale

WA is characterized by large aerosols loading as a result of biomass burning during farming season and the natural influence of the harmattan dust via the north-east winds. The aerosol emissions and transport are still affected by large uncertainties. Seeking solutions to the uncertainties via the application of numerical models only have been shown to be inadequate on its own. The greatest of the uncertainties is the influence of climatic change to aerosols transport [31]. In the macro scale analysis, we consider what happens in both the PBL and the free atmosphere because they interchangeably influence each other [5, 32]. The aerosol concentrations used to analyze in Eq. (2) are fixed to zero at the domain boundaries. This step is to allow for the external incoming aerosol amount to be minute at the sources. Since, this assumption is important to simultaneously determine both the vertical and horizontal profile of the atmosphere; there still exists the uncertainty caused by wind recirculation that takes place at the boundary of the PBL and free troposphere. Therefore the Neumann boundary condition is applied to obtain the physics of the aerosols physical tendency during transportation. Mayya et al. [18] adopted the Neumann boundary condition to analyze particles undergoing turbulent diffusion near absorbing surfaces e.g. PBL. Hence we must know the extent of influence the two media, that is, PBL and free tropo sphere has on the aerosols transport. The volume of pollutant dispersed from its various sources across WA is assumed to possess the same characteristics as shown in Fig. 5 i.e. large volume of diffusing pollutants concentrate at about 100 m above its dispersion source. This idea is drawn from the fact that aerosols may be radioactive and nonradioactive [1, 33]. Hence the assumption that particles possess the same characteristics is scientifically viable since the particles are in motion. The maximum range of the diffusing particulates at a maximum speed of 5 m/s is about 100 m. The volume of pollutant at this point is very low (Fig. 5(a)). At macro scale dispersion (Fig. 5(b)), the same characteristics shown in the micro scale transport is experienced. This further affirms that the radioactive or nonradioactive state has no adverse effect on the aerosols transport. The difference between the micro and macro scale is that the maximum speed of the macro scale is less than 4.4 m/s. This low speed enables the pollutants to acquire maximum range of about 15 km. Fig. 6 shows the aerosol transport within four years. The red colour depicts region of very dense aerosol particulates, the yellow colour shows the region of dense aerosol particulates, and grey colour shows region of light dense aerosol particulates. A comparative study with satellite observation in Fig. 6 shows that the type of aerosol in Fig. 6(b) and Fig. 6(d) can be classified by their peculiar transport (y-direction) as made-up of dust, smoke, soot, etc. This result agrees with the peculiar transport of mainly dust [10] or smoke [34] which has been investigated. The implication of this result is that atmospheric aerosol could build-up with time. If the aerosol is of higher lifetime, the aerosols transport has the tendency of shifting farther than its source of dispersion. The TOMS AI observation for January of 2000-2003 of WA (shown in Fig. 6) affirm the shifting tendency of built-up aerosol travelling at low speed. This type of aerosol is known to absorb ultraviolet (UV) rays. UV absorbing aerosol is dependent on the altitude, hence, the higher the aerosol altitude, the greater the fraction of affected molecular radiation. In view of this research, the UV absorbing aerosols might be affected by the northeast monsoon, rapid chemical transformations and aerosol removal processes.

The shift from the red arrow in 2000 southward and its continuous glaring shifts (the blue arrow) in 2001, 2002 and 2003 affirmed the macro scale functionality of the model. Though it will be quick to affirm that the shift was due to the global climate teleconnections (GCT), however, the science at which this aerosols

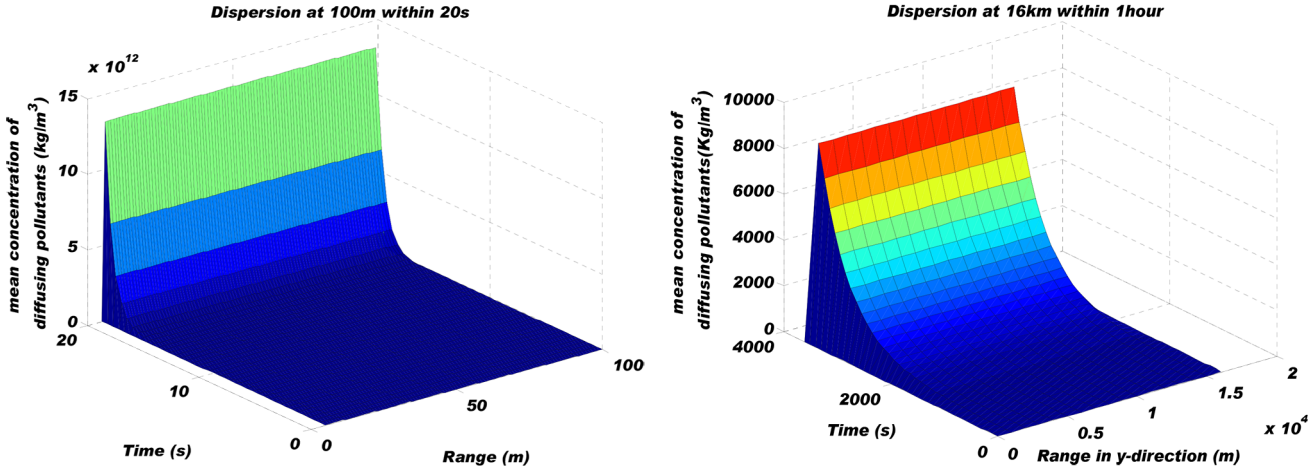

Fig. 5. Micro scale analysis of diffusing pollutants.

shift towards the coastal belt is quite unique and may not be explained using the aerosols micro-scale transport. GCT includes climatic oscillations and regional climate systems. The climatic oscillation includes El Nino-Southern Oscillation and North Atlantic Oscillation. The North Atlantic Oscillation originates eastward from the southwestern North Atlantic to Portugal and West Africa. Therefore, there exists another explanation with respect to the aerosols transport alongside the gradual annual shift of the aerosol due to GCT. A further analysis on the y-axis transported as viewed by the satellite sensor (Fig. 6) would enable us to understand the physics of the aerosol transport with respect to the changing angular satellite imagery capture.

We assume that if the moving aerosol is viewed from the satellite sensor that is relatively moving at the earth's rotational speed, it will experience multiple refractive indexes which affect the actual measurement of the AOD. In Fig. 7, the satellite sensor has the challenge of evaluating the right refractive index of a moving aerosol. If we adopt the results from literature [25] for the x-direction transport-where the aerosol travels at a speed of 4.4 m/s, then the illustration in Fig. 8 can be easily evaluated.

We propose that the number refracting angle depends on the type of aerosols, its speed and the incident angle of the satellite sensor. Let us assume that three refracting angles of the signal are α, β, and γ. Hence from the basic of refractive index

$$\left.\begin{aligned}\sin\frac{\theta}{2}&=n_1\cos\alpha\\ \sin\frac{\theta}{2}&=n_2\cos\beta\\ \sin\frac{\theta}{2}&=n_3\cos\gamma\end{aligned}\right\} \tag{21}$$

If the trigonometric rule $\left[\sin\theta=\left(\sin\frac{\theta}{2}+\sin\frac{\theta}{2}\right)\cos\frac{\theta}{2}\right]$ is applied for a full incident angle from the sensor, then

$$\sin\theta=n_1\cos\alpha\cos\frac{\theta}{2}+n_2\cos\beta\cos\frac{\theta}{2} \tag{22}$$

Since the relative air mass of a typical sunphotometer is written as $m=\frac{1}{\sin(\theta)}$, then the concentration of pollutants (C) can be expresses as

$$n=\frac{C}{\sin(\theta)} \tag{23}$$

If Eq. (9) is substituted into Eq. (8), then

$$C=n^2\cos\alpha\cos\frac{\theta_i}{2}+n^2\cos\beta\cos\frac{\theta_1}{2}+\ldots\ldots\ldots\ldots n^2\cos\gamma\cos\frac{\theta_n}{2} \tag{24}$$

If we compare each terms at the right of Eq. (24) and the right term of Eq. (4), it would be easy to affirm that several dispersion sources determine the complexity of measuring the AOD using the satellite sensor - MISR. The AERONET ground data available on http://aeronet.gsfc.nasa.gov/ for AOD was compared with the satellite data set for Lagos, Nigeria (Fig. 9) for 2011 and 2013. The monthly average AOD data set of both the satellite and ground stations were obtained and plotted as shown in Fig. 9. The statistical analysis shown in Table 3 further affirms our guess on the actual aerosols dispersed from the earth and the migrated aerosols in the tropopause and stratosphere.

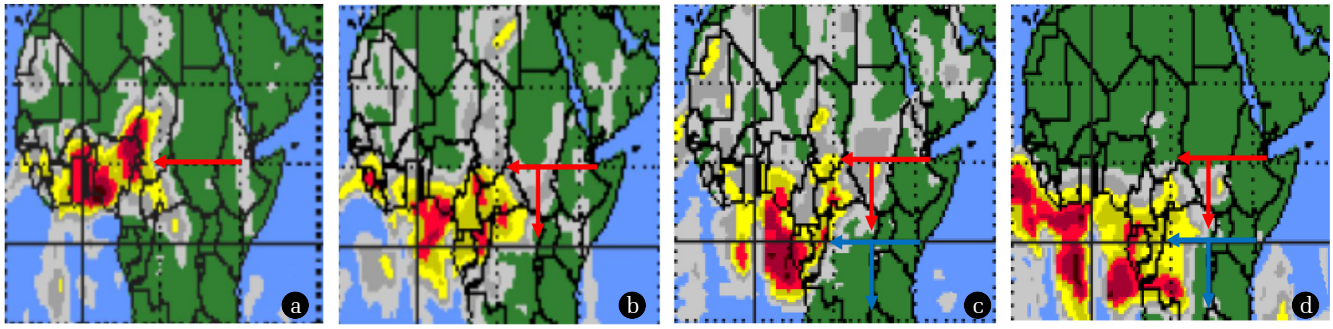

Fig. 6. (a) Shift January 2000 (b) Shift January 2001 (c) Shift January 2002 (d) Shift January 2003.

Table 3. Statistical Analysis of Ground and Satellite Data Set

Statistical Parameter	2012		2013	
	Ground	Satellite	Ground	Satellite
Standard error	0.03194	0.074879	0.049783	0.06908
95% confidence interval	0.075539	0.169377	0.10957	0.15391
Variance	0.008162	0.056069	0.02974	0.052492
Standard deviation	0.090341	0.236789	0.17245	0.229112
Coefficient of variation	0.089	0.5213	0.19466	0.54109
Skew	-0.205	1.03	0.504	0.904
Kurtosis	-1.009	-0.298	-0.975	-0.434
Kolmogorov-Smirnov stat	0.15	0.245	0.233	0.265

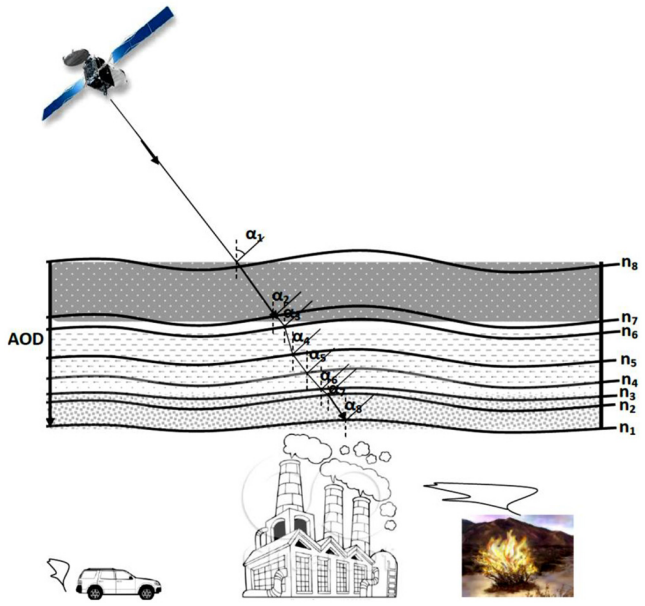

Fig. 7. Illustration of the retrieval.

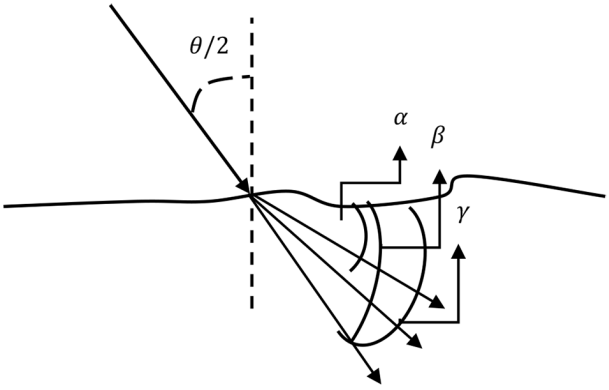

Fig. 8. Moving effect of aerosols on refractive indexes.

The two evidences, that is, analytical and field observation affirms the complex nature of aerosols which depends on the geographical location. The micro scale analysis of the range in y-direction reveals that aerosol distribution over the PBL sub-layers showed disturbances at lower range and higher disturbances at higher range. In Fig. 10(a), the possibility of obtaining strange aerosol distribution especially when they begin to coagulate via inelastic collision was expressed. The perturbative nature as shown in the 3D micro scale analysis further corroborate the wind re-circulation effect on aerosols content and rain formation [35]. For example, Fig. 6(a) and Fig. 6(c), that is, in the year 2000 and 2002 showed the intermittent aerosol distribution towards Liberia Sierra Leone, Guinea respectively. The magnitude of the aerosols loading at this differs as the major volume shifts off the coast towards Cape Verde. This phenomenon is numerically illustrated in Fig. 10(b). The wind pattern and the convective activities near the coastal ties may be partly responsible for the aerosols loading extension.

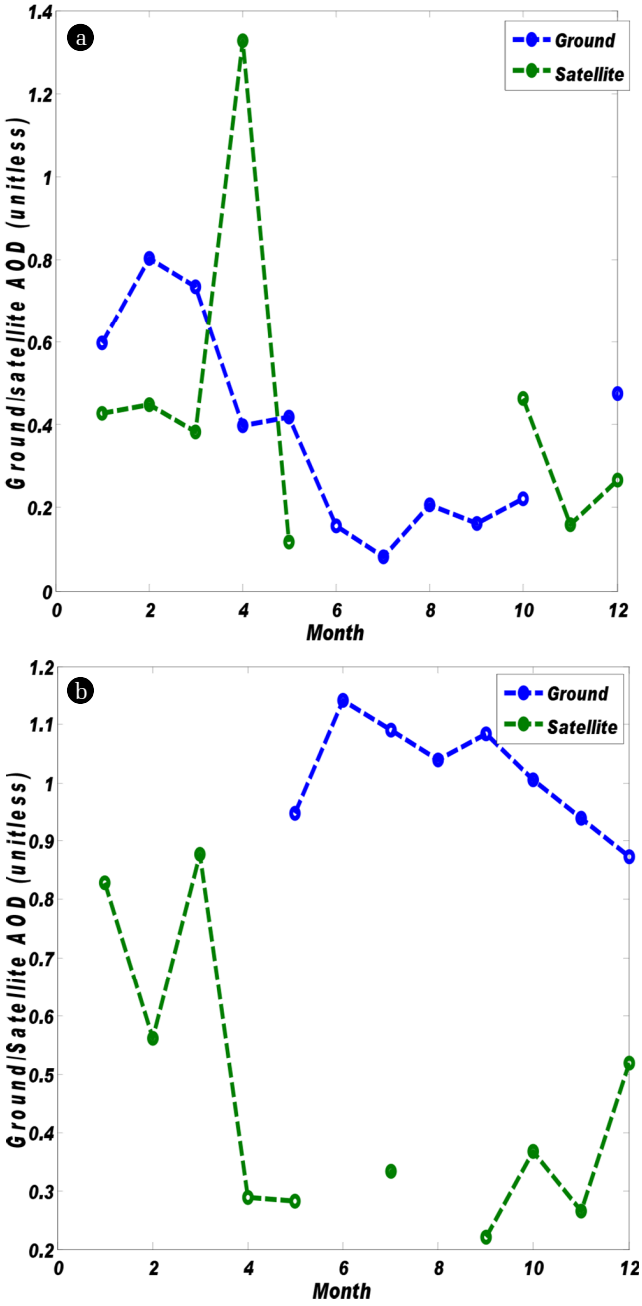

Fig. 9. Ground and satellite observations over Lagos.

The lifetimes of the aerosols dispersed in the y-direction in 2002 may be below a year (Fig. 6(c)). The macro scale analysis of the aerosol distribution in Fig. 11(a) and Fig. 11(b) showed that the aerosols loading is more dependent on the space than time in the y-direction. This is also affirmed in Fig. 6(a) - Fig. 6(d). We propose that though the possibility that collisions of aerosols may reduce their number concentration, however, it does not affect the conservation of the total particulate mass. This idea can be affirmed by the numerical simulations in Fig. 9(a) and Fig. 9(b).

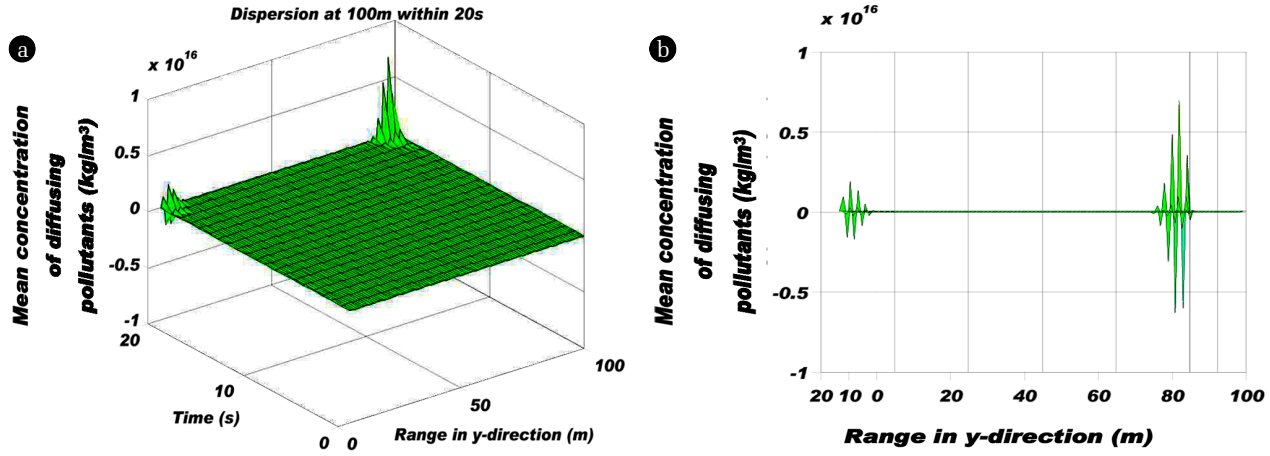

Fig. 10. (a) 3D micro scale analysis (b) 2D micro scale analysis.

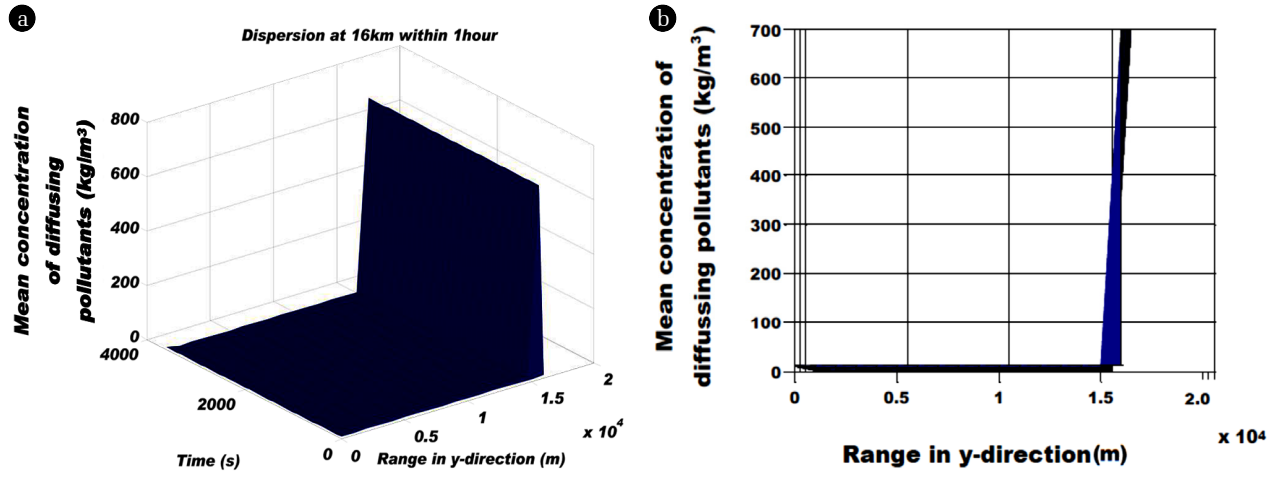

Fig. 11. (a) 3D micro scale analysis (b) 2D micro scale analysis.

In literature, atmospheric circulation pattern in the four climatic zones in WA zones is controlled by some salient factors like AEJ, ITCZ, ITD, associated HL, STJ, troughs and cyclonic centers associated with AEW and TEJ. AEJ operates at mid troposphere (600-700 mb) with maximum wind speed above 10 m/s and travels to WA from the East Africa (Andres et al., 2009). ITCZ also contributes to the convective rainfall pattern via the south-north-south displacement. The numerical prediction (Fig. 8(b)) shows that the aerosols loading could travel 15-17 km within an hour under the set condition.

5. Conclusions

The mode of aerosols transport within the lower atmosphere of WA has been described. The dispersion model was used to study aerosols content dynamics expected in a virtual stokes regime. The mean concentration diffusion of aerosols was higher in the micro-scale site. The difference between the micro and macro scale sites is that the maximum speed of the macro scale is less than 4.4 m/s. This low speed enables the pollutants to acquire maximum range of about 15 km. The multiple refractive indexes created by the thick heterogeneous aerosols layer in the atmosphere were proven to create a strange transport pattern over WA. It was also discovered that the build-up of the purported strange transport pattern with time has enormous potential to influence more climatic change effects in the long term. Even when the AEJ drives the aerosols layer at about 10 m/s, the interacting layers of aerosols are compelled to mitigate its speed to about 4.2 m/s on macro scale level and boost its speed at 30 m/s on the micro scale level.

The mean concentration diffusion of aerosols also affirmed that meteorological influences were one of the driving force of aerosols transport in WA. Also it was proven that the multiple refractive indexes compromise the accuracy of the satellite sensor in determining the AOD of an area. The coagulation processes of aerosols via inelastic collision do not affect the conservation of the particulate mass per time. Hence if the layer of aerosols travels at about 15 km/h in the macro scale settings, then the 3D particulate transport can be adjudged to be very perfect.

The study recommends that there should be an urgent need to embark on massive information driven project in WA. Active

participation of the government of the WA countries and an uncompromised synergy of all funded projects within the region might help avert or mitigate meteorological accidents in the future. This result of this study is also relevant in the tropical region of India and Malaysia to prevent a reoccurrence of the excessive heat flux that claimed life-forms in India.

Acknowledgements

The author appreciates the sponsorship of Covenant University, Nigeria. The author declares that there is no conflict of interest regarding the publication of this paper. The author is grateful to Akinyemi ML and Akin-Ojo O.
Authors Contribution: Emetere designed and wrote the project.

References

1. Emetere ME, Akinyemi ML. Modeling of generic air pollution dispersion analysis from cement factory. *Analele Universitatii din Oradea–Seria Geografie* 2013;23:181-189.
2. Emetere ME. Modeling of particulate radionuclide dispersion and deposition from a cement factory. *Ann. Environ. Sci.* 2013;7:71-77.
3. Uno I, Wang Z, Chiba M, et al. Dust model intercomparison (DMIP) study over Asia: Overview. *J. Geophys. Res.* 2006;111: D12213.
4. Sun WY, Yang KJS, Lin NH. Numerical simulations of Asian dust-aerosols and regional impacts on weather and climate - part II: PRCM-dust model simulation. *Aerosol Air Qual. Res.* 2013;13:1641-1654.
5. Emetere ME, Akinyemi ML, Akinojo O. Parametric retrieval model for estimating aerosol size distribution via the AERONET, LAGOS station. *Environ. Pollut.* 2015;207:381-390.
6. Sun WY. Conserved semi-lagrangian scheme applied to one-dimensional shallow water equations. *Terr. Atmos. Ocean. Sci.* 2007;18:777-803.
7. Habib G, Venkataraman C, Chiapello I, Ramachandran S, Boucher O, Reddy MS. Seasonal and interannual variability in absorbing aerosols over India derived from TOMS: Relationship to regional meteorology and emissions. *Atmos. Environ.* 2006;40:1909-1921.
8. Sun WY, Yang KJS, Lin NH. Numerical simulations of Asian dust-aerosols and regional impact on weather and climate - part I: Control case-PRCM simulation without dust-aerosols. *Aerosol Air Qual. Res.* 2013;13:1630-1640.
9. Benson DA, Wheatcraft SW, Meerschaert MM. Application of a fractional advection-dispersion equation. *Water Resour. Res.* 2000;36:1403-1412.
10. Dudhia J, Gill D, Manning K, et al. PSU/NCAR mesoscale modeling system tutorial class notes and user's guide: MM5 modeling system version 3. Boulder, CO: NCAR; 2003.
11. Cheng FY, Byun DW, Kim SB. Sensitivity study of the effects of land surface characteristics on meteorological simulations during the TexAQS2000 period in the Houston-Galveston area. In: 13th PSU/NCAR Mesoscale Model Users' Workshop; 10-11 June; Boulder, CO; 2003.
12. Doraiswamy P, Hoegrefe C, Hao W, Civerelo K, Ku JY, Sistla G. A retrospective com-parison of model based forecasted PM2.5 concentrations with measurements. *J. Air Waste Manage. Assoc.* 2010;60:1293-1308.
13. Vladutescu DV, Wu Y, Gross B, Moshary F, Ahmed S. Optical properties of aerosols and their sensitivity to relative humidity and size distribution in the New York City urban-coastal area. *EARSeL eProceedings* 2012;11:52-63.
14. Emetere ME, Akinyemi ML, Akin-Ojo O. Aerosol optical depth trends over different regions of Nigeria: Thirteen years analysis. *Mod. Appl. Sci.* 2015;9:267-279.
15. Madala S, Satyanarayana A, Prasad V. Micro-scale dispersion of air pollutants over an urban setup in a coastal region. *Open J. Air Pollut.* 2012;2:51-58.
16. Cazacioc LV, Cazacioc A. Impact of the macro-scale atmospheric circulation on snow cover duration in Romania. *Croat. Meteorol. J.* 2005;40:495-498.
17. Gbadebo AM, Amos AJ. Assessment of radionuclide pollutants in bedrocks and soil ewekoro cement factory, Southwest Nigeria. *Asian J. Appl. Sci.* 2010;2010:1-10.
18. Mayya YS, Tripathi SN, Khan A. Boundary conditions and growth of mean charges for radioactive aerosol particles near absorbing surfaces. *Aerosol Sci.* 2002;33:781-795.
19. Johar RS, Scholz PD. The effect of aerosol temperature and particle number density on light scattering. *Atmos. Environ.* 1970;4:633-637.
20. Lead C. Aerosols, their direct and indirect effects [Internet]. c2015 [cited 12 December 2015]. Available from: www.grida.no/climate/ipcc_tar/wg1/pdf/tar-05.pdf.
21. McKibbin R. Mathematical modeling of aerosol transport and deposition: Analytic formula for fast computation. In: Proc. iEMSs 4th Biennial Meeting – Int. Congress on Environmental Modelling and Software: Integrating sciences and information technology for environmental assessment and decision maing. iEMSs; 2008. p. 1420-1430.
22. Massabo M, Catania F, Paladino O. A new method for laboratory estimation of the transverse dispersion coefficient. *Ground Water* 2007;45:339-347.
23. Egan Tony. Conversion from constant flow system to variable flow. 2015 armstrongfluidtechnology.com/.../94-21_conversionfrom constanttovaria. (retrieved 12th December, 2015)
24. de Gouw JA, Warneke C, Stohl A, et al. Volatile organic compounds composition of merged and aged forest fire plumes from Alaska and western Canada. *J. Geophys. Res.* 2006;111:D10303.
25. Lovejoy ER, Curtius J, Froyd KD. Atmospheric ion-induced nucleation of sulphuric acid and water. *J. Geophys. Res.* 2004;109:D08204.
26. Yermakov AN, Larin IK, Ugarova AA, Purmal AP. Iron Catalyst of SO_2 oxidation in the atmosphere. *Kinet. Catal.* 2003;44:476-489.
27. Pausata FSR, Gaetani M, Messori G, Kloster S, Dentener FJ. The role of aerosol in altering North Atlantic atmospheric circulation in winter and its impact on air quality. *Atmos. Chem. Phys.* 2015;15:1725-1743.
28. Drewnick F, Hings SS, Alfarra MR, Prevot ASH, Borrmann

S. Aerosol quantification with the Aerodyne Aerosol Mass Spectrometer: Detection limits and ionizer background effects. *Atmos. Meas. Tech*. 2009;2:33-46.
29. Olaleye VF, Oluyemi EA, Akinyemiju OA. Environmental disamenities produced by particulate and gaseous emissions from Ewekoro cement kilns on some strata of aquatic and terrestrial ecosystems. *J. Appl. Sci*. 2005;5:428-436.
30. Akinyemi ML, Emetere ME, Akinwumi SA. Dynamics of wind strength and wind direction on air pollution dispersion. *Asian J. Appl. Sci.* 2016;4:422-429.
31. Andres-Hernandez MD, Kartal D, Reichert L, et al. Peroxy radical observations over West Africa during AMMA 2006: Photochemical activity in the outflow of convective systems. *Atmos. Chem. Phys.* 2009;9:3681-3695.
32. Emetere ME. A model for analyzing temperature profiles in pipe walls and fluids using mathematical experimentation. *Adv. Mech. Eng.* 2014;2014:490302.
33. Rajeev K, RamanathanV, Meywerk J. Regional aerosol distribution and its long-range transport over the Indian Ocean. *J. Geophys. Res.* 2000;105:2029-2043.
34. Vakkari V, Kerminen VM, Beukes JP, et al. Rapid changes in biomass burning aerosols by atmospheric oxidation. *Geophys. Res. Lett*. 2014;41:2644-2651.
35. Valipour M. Optimization of neural networks for precipitation analysis in a humid region to detect drought and wet year alarms. *Meteorol. Appl.* 2016;23:91-100.